Electrical Power and Energy Systems 104 (2019) 807–816

Contents lists available at ScienceDirect

Electrical Power and Energy Systems

journal homepage: www.elsevier.com/locate/ijepes

Control strategy for AC-DC microgrid with hybrid energy storage under different operating modes

Narsa Reddy Tummuru[a,*], Ujjal Manandhar[b], Abhisek Ukil[c,*], Hoay Beng Gooi[b], Sathish Kumar Kollimalla[b], Swami Naidu[b]

[a] School of Computing and Electrical Engineering, Indian Institute of Technology Mandi, Himachal Pradesh 175005, India
[b] School of Electrical and Electronic Engineering, Nanyang Technological University, 50 Nanyang Avenue, Singapore 639798, Singapore
[c] Dept. of Electrical & Computer Engineering, 20 Symonds Street, 1010 Auckland, New Zealand

ARTICLE INFO

Keywords:
Battery
Dynamic energy management
Hybrid energy storage
Microgrid
Power quality
Supercapacitor

ABSTRACT

In this paper, a control strategy is proposed for renewable-interfaced hybrid energy storage system (HESS) under grid connected/islanding conditions. A second harmonic based phased locked loop (PLL) is employed for effective synchronization/resynchronization of the microgrid system under contingency conditions. The operation and management of the microgrid system under both these modes are accomplished by an efficient adaptive power management algorithm. A quantitative analysis on the HESS performance is provided in order to investigate the effectiveness of the proposed approach. Further, small signal average models are derived to comment on the system stability. This approach address seamless transfer between the various sub-modes of the system along with additional services such as power quality enhancement and power dispatch between various sources. The effectiveness of the proposed scheme is verified by both simulation and experimental investigations.

1. Introduction

The stochastic nature of renewable energy sources (RES) coupled with the unpredictable changes in the load, demands hybrid energy storage systems (HESS) (such as batteries, supercapacitors etc.,) in the present day microgrids [23,6,16]. The HESS support the renewable energy producers and also system operators by providing many ancillary services [12]. From the control perspective, the hybrid microgrids (RES interfaced HESS) are classified into grid-interfaced and standalone configurations. The stochastic nature of these RESs raise many technical issues while operating in grid-interfaced and islanded modes [6,5,17]. In addition, the transition from one mode to another and vice versa, is an important aspect that need to be considered while design of suitable management schemes for reliable and continuous operation of these hybrid microgrids.

1.1. Literature review

The energy management schemes (EMS) reported in Lu et al. [13] extracts powers from the PV source, battery and supercapacitor, based on the states of each of the individual source. However, the power quality aspects on the ac side have not been addressed in their work. The EMS based on model-predictive control reported in Hredzak et al. [8] is limited to supercapacitor-battery hybrid in a DC microgrid environment by assuming a constant DC link voltage. Moreover, this classical model predictive control relies on a discrete model of the control system and a cost function, making it computationally intensive. Similar performance as obtained in Hredzak et al. [8]is achieved using a much simpler EMS reported in Hredzak et al. [7] making it amenable to be implemented using normal controllers.

The micro grid voltage source converter (VSC) changes its management philosophy based on the connection/disconnection status of the micro grid to the utility grid [15,4]. This mode change in the VSC's management philosophy is decided by islanding detection method. Islanding detection schemes can be divided into distant and native modules. Distant methods rely on communication networks between microgrid and utility [3] leading to high cost along with complexity. On the other hand, native module comprising passive and active methods use local measurements information at the point of common coupling (PCC) [15]. The active islanding techniques intentionally introduce disturbances at the output of the VSC's to find if they affect the voltage, frequency, or impedance parameters, in such case it is assumed that the grid has been disconnected and the VSC is isolated from the load. Moreover, active methods introduce a disruption and force wider

* Corresponding author.
E-mail addresses: narasaiitm@gmail.com (N.R. Tummuru), ujjal001@e.ntu.edu.sg (U. Manandhar), a.ukil@auckland.ac.nz (A. Ukil), ehbgooi@ntu.edu.sg (H.B. Gooi), skollimalla@ntu.edu.sg (S.K. Kollimalla), nksn@ntu.edu.sg (S. Naidu).

https://doi.org/10.1016/j.ijepes.2018.07.063
Received 19 September 2016; Received in revised form 7 March 2018; Accepted 26 July 2018
Available online 07 August 2018

changes of the parameters after islanding event. Therefore, islanding event can be distinguished even under small power perturbations.

Voltage drifting methods mainly use the under/over voltage information at the PCC and the respective relays initiate the islanding event [20,9]. In few of frequency drifting schemes, the autonomous system is enforced by moving the PCC frequency outside permissible frequency limits. Active frequency drift [22], Sandia frequency shift [19] and imaginary power variation [24] are the some of key frequencies drifting methodologies. On the other hand, several methods have been proposed in the literature by creating perturbations without affecting the stability of the system [2,18,11,10]. However, these methods degrade the power quality of the system.

1.2. Objective of the study

In this paper, a simple unified management philosophy is proposed to provide uninterrupted supply to the load under grid connected and islanded conditions. The proposed scheme uses a harmonic current injection method that detects islanding event without affecting the microgrid stability and also, enhances the power quality.

The main features obtained from the proposed scheme are:

- An effective power flow management at the DC link.
- Improved power quality features at the point of common coupling under grid connected mode due to the attenuation of 2nd harmonic of PCC voltage.
- Allows inherent current limits for both supercapacitor and battery units.
- Seamless mode transfer between different modes.
- The islanding event can be detected in a short time by comparing an exponential raise in second harmonic of PCC voltage with a suitable threshold [as shown in Figs. 4 and 14].

In this paper, system configuration and proposed control strategy are described in Section 2. Quantitative analysis on various functionality is described in Section 3. In Section 4, the stability analysis under various modes is presented. Some of the results and discussion are described in Section 5. Finally, concluding remarks are presented in Section 6.

2. Hybrid AC-DC microgrid configuration and proposed control strategy

The hybrid microgrid mainly consists of AC and DC microgrids connected through controlled power electronic interfaces, as illustrated in Fig. 1. A three-phase four-wire split capacitor VSC topology is used on the AC side to exchange power between the AC and DC microgrids effectively.Non-linear and unbalanced loads are connected on the AC side, in order to test the additional capabilities of the proposed scheme such as harmonic compensation, reactive power support, load balancing and power factor correction under grid connected mode. A circuit breaker (CB) is used to isolate the utility grid from hybrid microgrid under contingency conditions. On the DC grid side, a photovoltaic (PV) system is connected through a boost DC-DC converter topology to extract peak power from the PV panels and HESS is used to balance the average and transient power flow at the DC grid. The AC-DC microgrid system considered in this paper is shown in Fig. 1 with following notations.

- v_B, v_{sc}, v_{dc} and v_g are the battery, supercapacitor, DC link and grid voltages.
- i_B, i_{sc}, i_{ld} and i_{vsc} are the battery, supercapacitor, DC load, and VSC currents.
- C_b, C_{sc}, C_{db}, C_{dsc}, C_{dc} and C_f are the battery, supercapacitor, DC link side battery, DC link side supercapacitor, VSC DC link and VSC filter capacitance's, and L_B, L_{sc}, L_f, R_L and R_{labc} are the battery, supercapacitor, VSC filter inductance of the DC and the AC side loads, respectively.
- S_a, S_b, S_c, S'_a, S'_b, S'_c, S_p, S_{1b}, S_{2b}, S_{1s} and S_{2s} are the control switches of VSC, PV converter, battery converter and supercapacitor converter, respectively.

A control strategy has been proposed in this paper for continuous operation of aforementioned microgrid under different operating modes as shown in Fig. 2. The transient and average powers are separated by a low pass filter and rate-limiter (RTL). These powers are fed to the islanding and grid power management (IPM & GPM) modules. The battery and supercapacitor management priorities are embedded in GPM and ISM modules respectively. The status of selector switches (SS1 & SS2) is decided by the islanding detection (ISD) algorithm and based on this signal the selector switch passes corresponding battery and supercapacitor reference values to control stages. The voltage source converter will change its mode of operation from grid interface/connected to islanding and vice versa based on activating signal from the ISD.

The details of aforementioned functional blocks in grid connected and islanding modes of the AC-DC microgrid are described in the following subsections.

2.1. Energy Storage Unit's Monitoring

The depth of discharge (DoD) status of the energy storage units is computed and monitored using the following mathematical equations [14].

$$DoD_j(t) = DoD_{oj} - \frac{1}{3600 N_{Cj}} \int i_j \, dt \tag{1}$$

where $j = B \text{ or } SC$, DoD_o, and N_C are the battery, supercapacitor, initial DoD of energy storage system (ESS) units and nominal capacity respectively. The computed DoDs of the battery and the supercapacitor units are fed to the IPM and GPM modules. Based on the status of the energy storage devices, the power management objectives are defined in these modules.

2.2. Islanding detection method and operating modes

The islanding detection method used in this work is shown in Fig. 3. Under grid connected mode, the voltage at the point of common coupling (PCC) is imposed by the utility grid, and its waveform is not altered by islanding detection algorithm. This grid voltage template is used for generation of VSC reference currents (i_r) under grid connected mode. Whereas, in case of islanding the PCC voltage follows the waveform of current injected by the voltage source converter [21] and the idea of this ISD algorithm is explained as follows,

A small perturbation is generated by modification in the phase signal of the phase locked loop (PLL) as shown in Fig. 3, so that the angle of VSC current reference is changed according to the following,

$$\theta_{vsc} = \theta + K \cos(\theta) \tag{2}$$

$$\cos(\theta_{vsc}) = \cos\{\theta + K \cos(\theta)\} \tag{3}$$

After simplification, the VSC reference current is given as follows,

$$\cos(\theta_{vsc}) \cong \cos(\theta) - \frac{K}{2} \sin(2\theta) \tag{4}$$

The islanding detection method is based on measuring second harmonic of the PCC voltage waveform and corresponding feedback signal (ϑ), control signal under change over from one mode to another are illustrated in Fig. 4. Fig. 4(a) shows the feedback (ϑ) and delayed signals from the ISD algorithm. At $t = t_1$, the grid is switched off. As a result, the feedback signal is more than ϑ_{min} and therefore, ISD algorithm sends activation signal to the CB as shown in Fig. 4(b). At $t = t_2$,

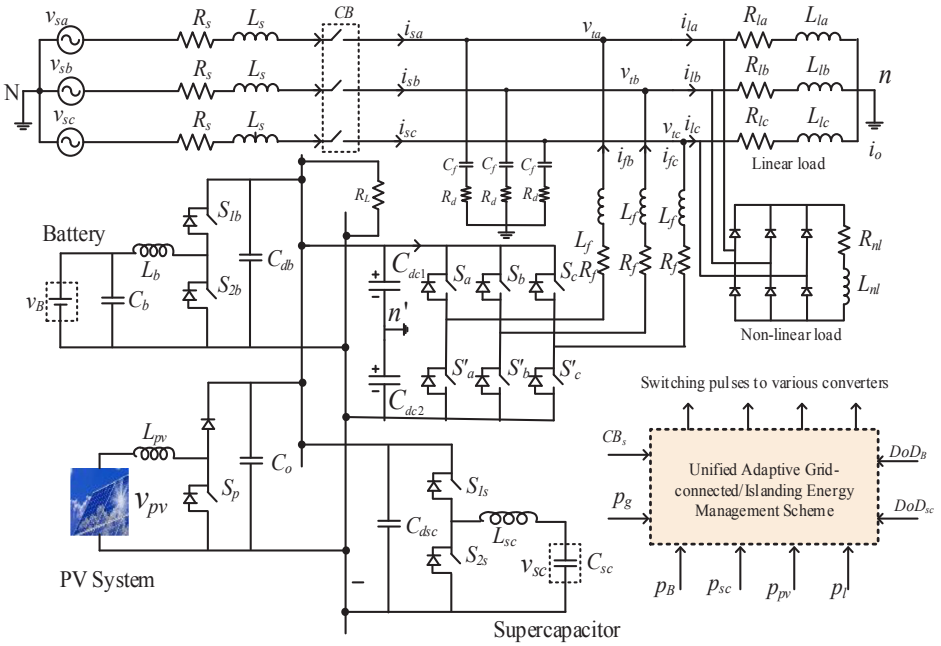

Fig. 1. AC-DC microgrid under consideration.

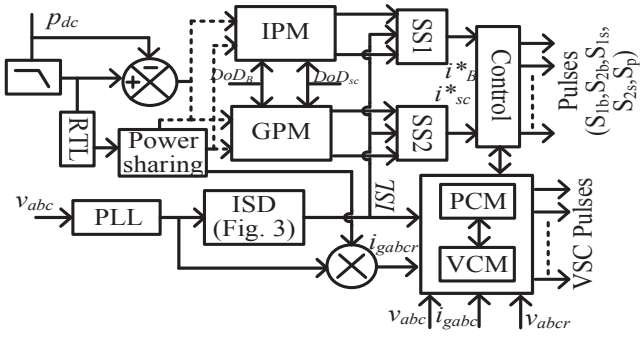

Fig. 2. Block diagram of microgrid proposed control system.

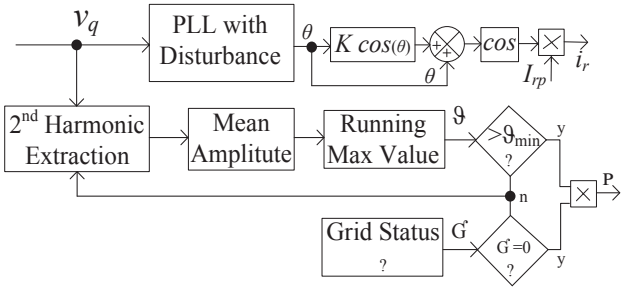

Fig. 3. Islanding detection algorithm.

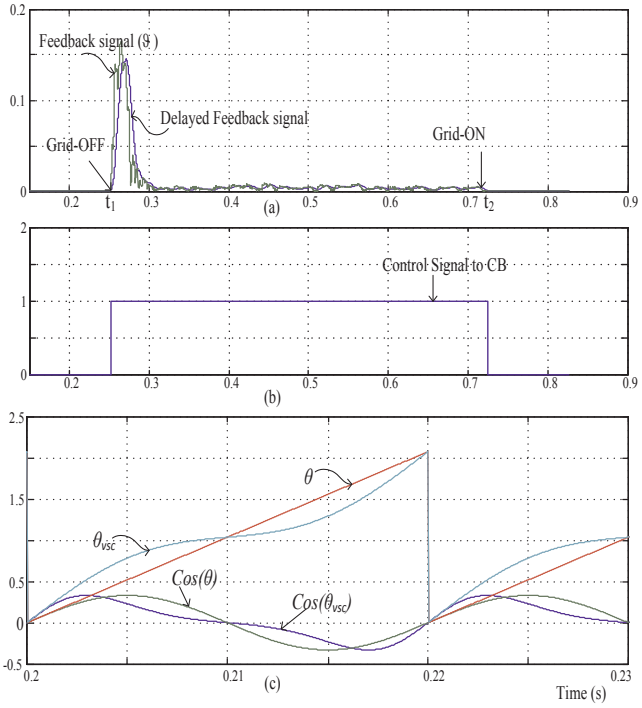

Fig. 4. (a) Feedback and delayed signals from islanded detection, (b) Control signal to CB, and (c) Phase waveform of the PLL and VSC current reference template at K = 0 [θ, Cos(θ)] and K = 0.8 [θ_{vsc}, Cos(θ_{vsc})].

the grid is reconnected and hence the feedback signal becomes zero. In this case, ISD algorithm sends deactivation signal to CB. The VSC current reference and phase of the PLL with $K = 0$ and 0.8 are illustrated in Fig. 4(c). The larger values of K will make the grid current non-sinusoidal and therefore, one has to select an appropriate value for effective operation of the system.

2.3. IPM and GPM Algorithms

The adaptive power management objectives are formulated to control various sources in the microgrid under islanding and grid connected scenarios as shown in Fig. 5. In Fig. 5, the variables S_{La}, S_{Ld}, M_{off}, fl_a, P_{ex}, P_{Ha}, ΔP_d, p_{pv}, p_g, p_{loss}, p_{sc}^*, p_B^*, p_{scr}, p_{Br}, λ, p_{ac}, p_{dcl} and P_{Hp} represent control signals for AC, DC loads, peak power deactivating module, floating condition, effective power, average power component, DC link power changes, PV power, grid power, losses, battery, supercapacitor references, supercapacitor rated power, battery rated power, sharing constant, AC, DC load powers, and peak power component respectively.

2.3.1. Islanding mode

The ESS plays a vital role under islanded conditions. The steady-

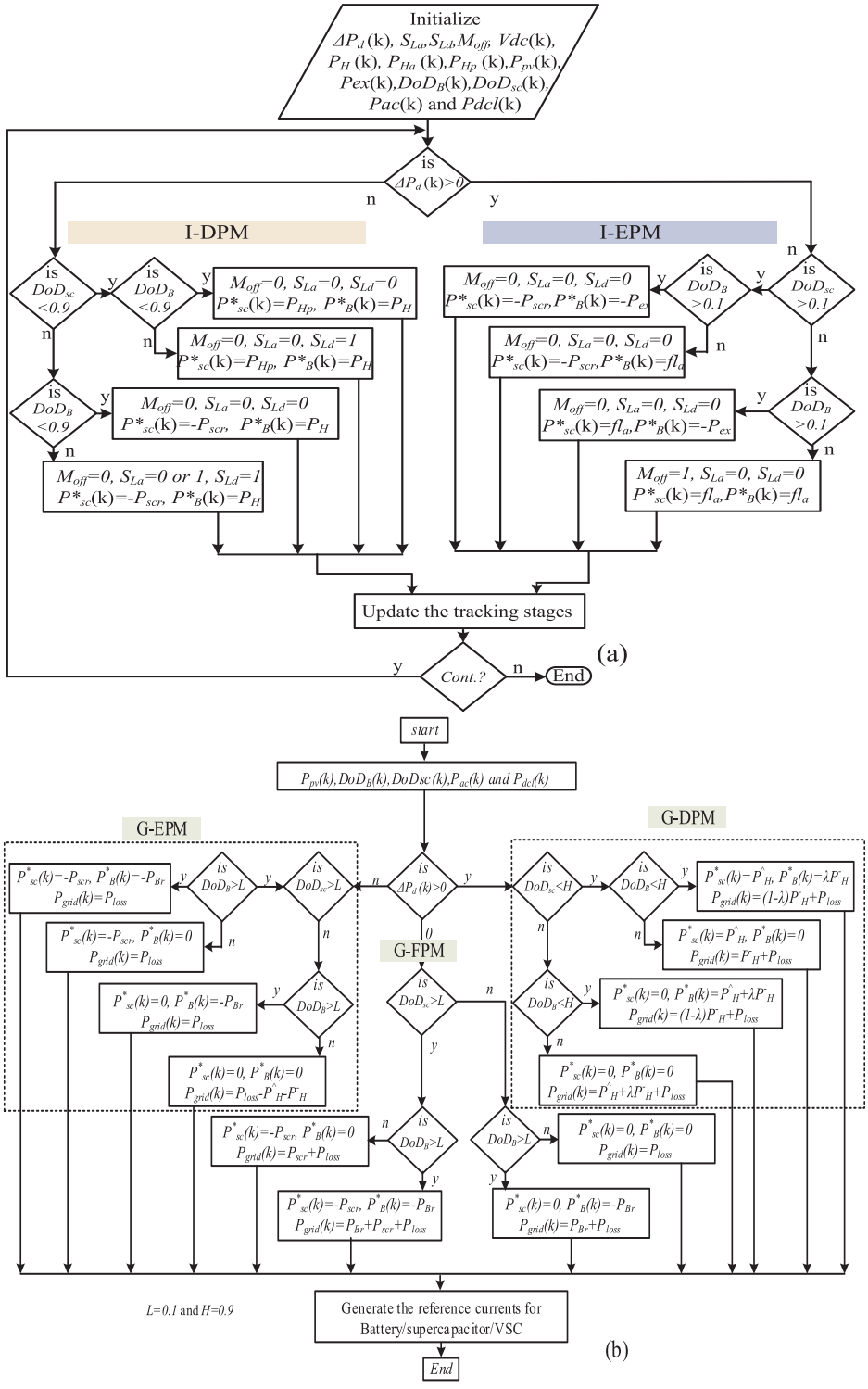

Fig. 5. (a) IPM and (b) GPM algorithms.

state and dynamic energy balance of the islanded microgrid should be regulated by energy storage system under renewable/load side disturbances. Based on the renewable power availability and load power requirement, two modes are identified under islanded conditions of AC-DC microgrid (i) islanded excess power mode (I-EPM) and (ii) islanded deficit power mode (I-DPM). The detailed description of the proposed islanded power management scheme under I-DPM is explained in the following subsection.

In an islanded excess power mode, mainly the PV system is used to share the load demand. The excess power is used to charge the battery and supercapacitor packs based on their DoD status. The supercapacitor continues to supply steady-state oscillatory and dynamic power components. The power management objectives under I-EPM are formulated in a flowchart as shown in Fig. 5(a). Similarly, the power management objectives are also defined for I-DPM as illustrated in the same figure.

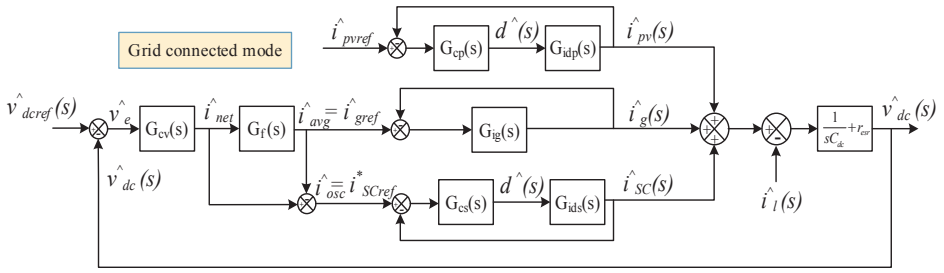

Fig. 6. Small signal average models under grid connected mode.

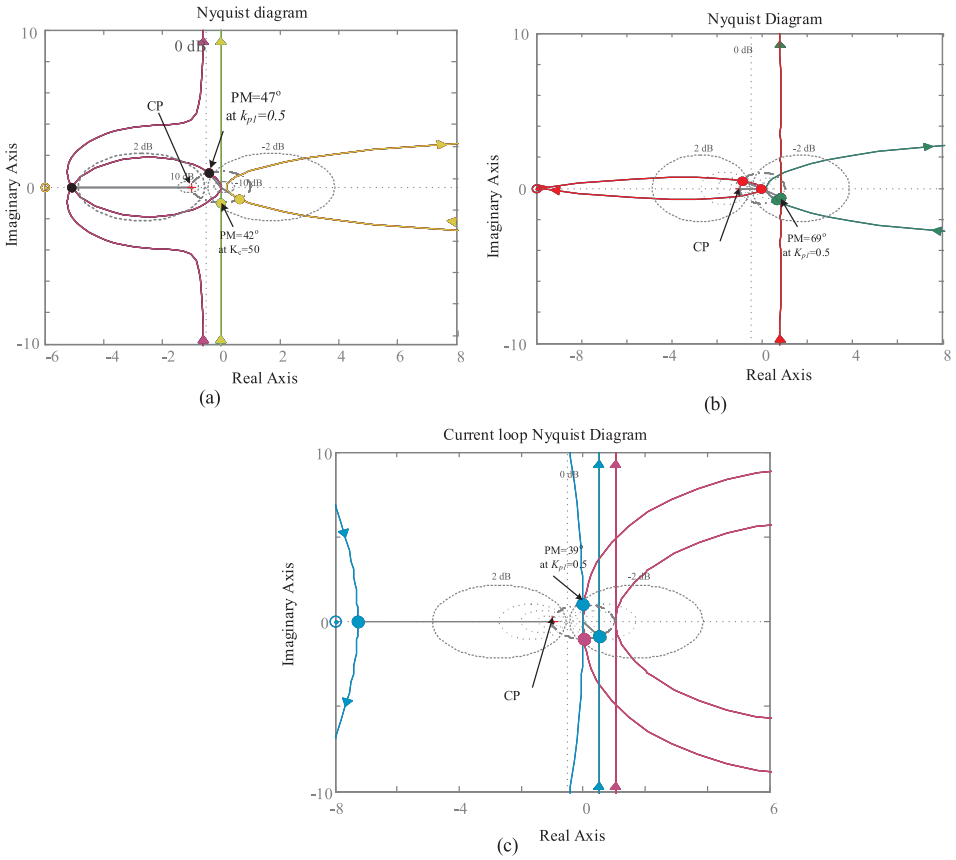

Fig. 7. Stability of the microgrid under various modes: (a) grid connected mode, (b) islanding mode, and (c) off-maximum power point tracking (MPPT) mode.

2.3.2. Grid connected mode

The ESS balances power flow in this mode. Based on the renewable power availability and load power requirement, three sub modes are identified in this mode (i) grid deficit power mode (G-DPM), (ii) grid excess power mode (G-EPM) and (iii) grid floating power mode (G-FPM). The power management priorities are programmed for various sources under this mode as shown in Fig. 5(b).

3. Various functionalities of proposed strategy

Various functionalities of the proposed control strategy are quantitatively analyzed in following section. High current rates $\left(\frac{di_B}{dt}\right)$ on the battery affect its internal resistance and available capacity. The change in internal resistance increases the losses [1]. These high current rates affect the battery performance in the long term. Using proposed strategy, these high current surges are diverted to supercapacitor and therefore, battery unit is free from high current rates. The quantitative analysis on the above aspects is given below,

3.1. DC link voltage dynamics

From the Fig. 1, the power balance at the DC link can be represented as follows,

$$p_{pv}(t) + p_B(t) + p_{sc}(t) + p_g(t) - p_l(t) = 0 \tag{5}$$

The change in energy at the DC link is given by,

$$\Delta W_{dc} = \frac{1}{2} C_{dc}(v_{dcr}^2 - v_{dc}^2) \cong v_{dcr} \Delta v_{dc} C_{dc}, \tag{6}$$

By combining the Fig. 15

$$\Delta v_{dc} = \frac{T}{C_{dc} v_{dcr}} \{p_{pv}(t) + p_B(t) + p_{sc}(t) + p_g(t) - p_l(t)\}, \tag{7}$$

In (7), T is AC cycle time period. The changes in renewable power/load will affect the dynamics in the DC link voltage. As a consequence, the transient power requirement at the DC link is supported by the supercapacitor units and the average power is shared by the battery and grid. Therefore, it ensures fast DC link voltage regulation.

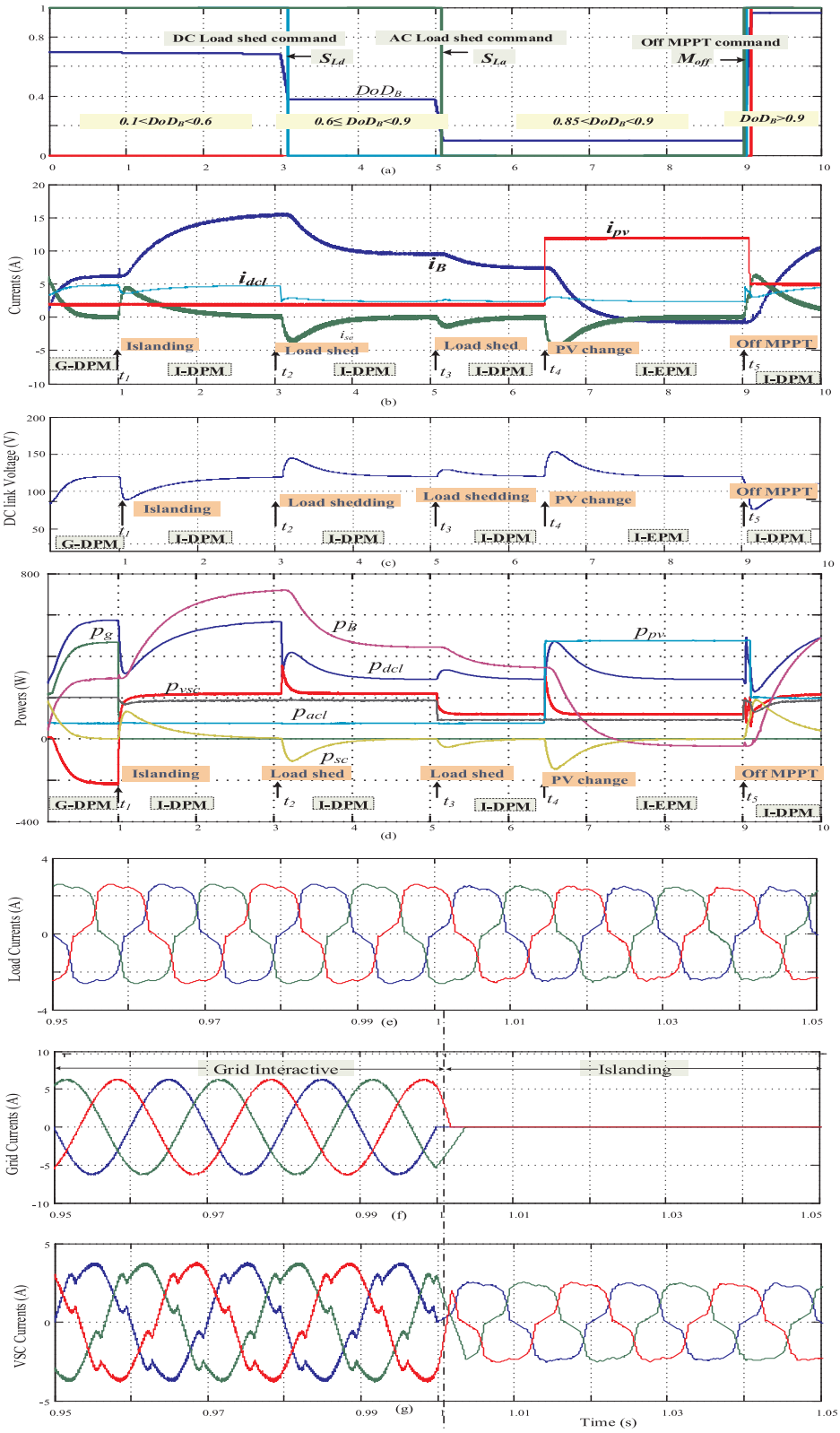

Fig. 8. Performance of proposed control strategy under grid interfaced and islanded conditions: (a) DoD of battery (b) PV current (i_{pv}), battery current (i_B), supercapacitor current (i_{sc}), and DC load current (i_{dcl}), (c) DC link voltage, (d) Average powers, (e) AC load currents, (f) grid currents and (g) VSC currents respectively.

3.2. HESS performance analysis

Corrosion will affect the internal resistance and available ampere-hour (*Ah*) capacity of the battery. The key parameters responsible for corrosion are battery voltage rates, acid concentration and temperature. High voltage rates increase corrosion. Corrosion and degradation reduce the available battery *Ah* capacity and herefore, a suitable energy management schemes are required to limit battery voltage and current rates in the grid interfaced/islanded modes. The change of internal resistance during one sampling step due to corrosion is given as follows,

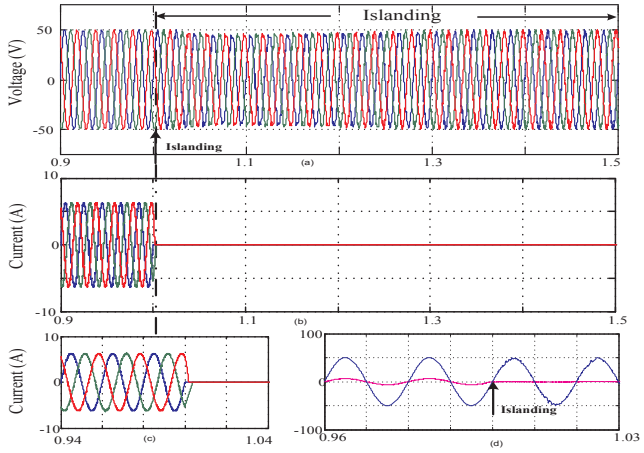

Fig. 9. Performance of proposed control strategy: (a) grid voltages, (b) grid currents, (c) enlarged view of grid currents and (d) grid voltage and current.

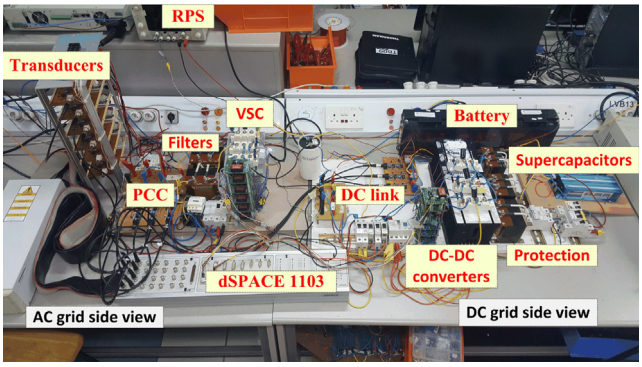

Fig. 10. Experimental setup.

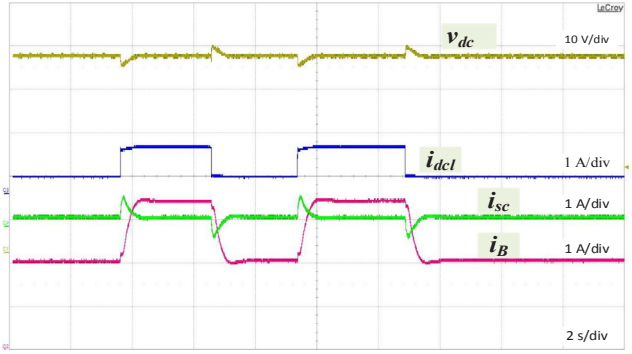

Fig. 11. DC grid side performance:DC link voltage (v_{dc}), DC load current (i_{dcl}), supercapacitor current (i_{sc}) and battery current (i_B).

$$r_k(t) = r_{lt}\left(\frac{\Delta w_t}{\Delta w_{lt}}\right); \quad r_{lt} = r_{d,e} - r_{d,0} \tag{8}$$

where r_{lt}, Δw_t, $r_{d,0}$ and Δw_{lt} are the limiting value of internal resistance, thickness of corrosion layer at t instant, initial resistance and limiting thickness of corrosion layer. The internal resistance at the end of life cycle of battery ($r_{d,e}$) can be written as,

$$r_{d,e} = \frac{C_N}{i_B}\{V_{ce} - V_0 + g_d(DoD_B)\} - \frac{x}{y} - r_{d,0} \tag{9}$$

where C_N, i_B, V_{ce}, V_0, g_d, DoD_B and M_d are the parameters of the Shepherd equation as defined in [1]. The variables $x = r_{d,0}M_d(DoD_B)$ and $y = C_{d,0} - DoD_B$.

The capacity reduction due to corrosion (Ah_k) is given as follows,

$$Ah_k(t) = \left\{Ah_{d,0} - DoD_B + \left(\frac{x_1}{y_1}\right)\right\}\left(\frac{\Delta w}{\Delta w_{lt}}\right) \tag{10}$$

where $x_1 = \frac{i_B}{C_N} r_{d,0} M_d\, DoD_B$, $y_1 = V_{ce} - V_0 + g_d\, DoD_B + r_d(t)\frac{i_B}{C_N}$ The capacity reduction due to degradation (Ah_{deg}) is given as follows,

$$Ah_{deg}(t) = Ah_{deg,lt}\; e^{-C_{zN}\left(1 - \frac{Z_{gN}}{Z}\right)} \tag{11}$$

The capacity reduction due to both corrosion (Ah_k) and degradation (Ah_{deg}) is given as follows,

$$Ah_d(t) = Ah_{d,0} - Ah_{d,k}(t) - Ah_{deg}(t) \tag{12}$$

The change of internal resistance and available Ah capacity of the battery for the proposed energy management scheme are computed using (11) and (12) and it is observed that the current stress on the battery is reduced with the proposed scheme (also illustrated in Fig. 11).

4. Stability analysis under different modes

To assess the stability of the system under various modes, the small signal average (SSA) models of the system are developed. The power converters are modulated in current control mode and modeled as controlled current sources.

Based on the grid status, DoD of HESS and renewable power availability, the following modes are identified in the microgrid such as (i) grid interfaced or grid connected mode: grid maintains the DC link voltage, (ii) islanded mode: battery maintains the DC link voltage and (iii) off-MPPT mode: PV maintains the DC link voltage. The derived SSA model under grid connected mode is illustrated in Fig. 6. In this analysis, $G_{cv}(s)$, $G_f(s)$, $G_{ig}(s)$, $G_{cs}(s)$, $G_{ids}(s)$, $G_{cp}(s)$ and $G_{idp}(s)$ are the small signal transfer functions of the DC link voltage controller, low pass filter, grid converter, supercapacitor current controller, supercapacitor converter in current control mode, PV current controller and PV converter in current control mode respectively. From Fig. 6, the loop gain transfer function can be derived as follows,

$$G_{cv}(s) = k_{p1} + \frac{k_{i1}}{s}, \quad G_f(s) = \frac{1}{1 + s\tau} \tag{13}$$

The closed loop transfer function of grid, supercapacitor current control are obtained as follows,

$$G_{igcl}(s) = \frac{k_{pgi}}{k_1 + k_3 k_{pgi}}, \quad G_{idscl}(s) = \frac{G_{cs}(s)G_{ids}(s)}{1 + G_{cs}(s)G_{ids}(s)} \tag{14}$$

Therefore, the loop gain of the system can be expressed as,

$$G(s)H(s) = G_{cv}(s)G_f(s)G_{igcl}(s) + (1 - G_f(s)) \times G_{idsccl}(s)\left(\frac{1}{sC_{dc}} + r_{esr}\right) \tag{15}$$

In (15), the gains $G_{cs}(s)$ and $G_{ids}(s)$ are expressed as,

$$G_{cs}(s) = k_{ps} + \frac{k_{is}}{s}, \quad G_{ids}(s) = \frac{s(C_{dc}V_{dc} + 2D'I_{Lsc})}{s^2 L_{sc}C_{dc} + s\frac{L_{sc}}{R_L} + D'^2} \tag{16}$$

In the above (13)–(16), the variables and k_{p1}, k_{i1}, τ, k_{pgi}, k_1 and D' represent proportional, integral constants of outer loop, time constant of LPF, inner loop proportional, integral constants and duty ratio of supercapacitor converter respectively.

The loop gain Nyquist plots are obtained using the above equations. The loop gain Nyquist contour should be on the right side of the critical point (CP) $(-1, 0)$ or within the unit circle under the event of dynamic transition from one mode to another. With the outer control loop gain (k_{p1}) as parameter, the stability of the microgrid under various modes are investigated and few of these frequency domain plots are shown in Fig. 7. The overall loop gain [$G_{lgg}(s)$] Nyquist plot under grid connected mode is shown in Fig. 7(a). At $k_{p1} = 0.5$, the system ensures stability,

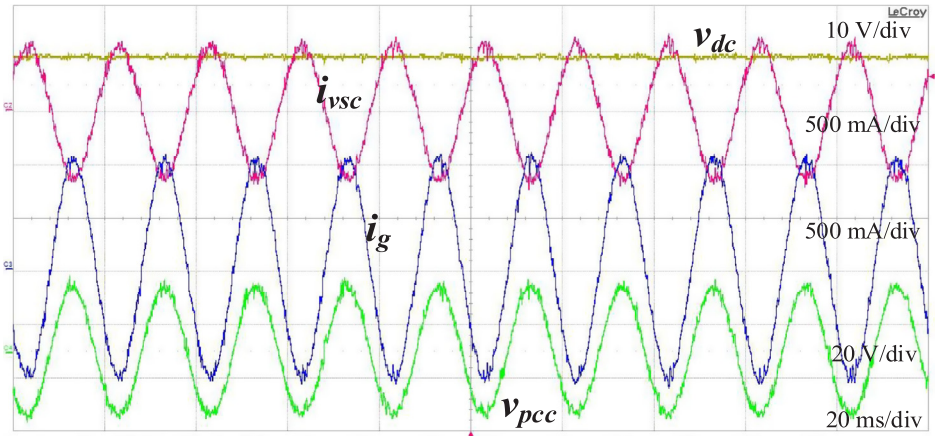

Fig. 12. Performance under grid connected mode:DC link voltage (v_{dc}), VSC current (i_{vsc}), grid current (i_g) and PCC voltage (v_{pcc}).

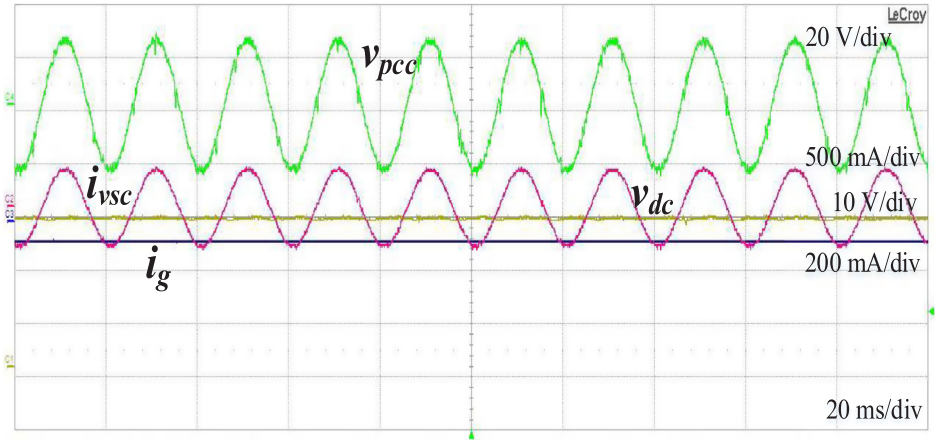

Fig. 13. Performance under islanding mode:DC link voltage (v_{dc}), VSC current (i_{vsc}), grid current (i_g) and PCC voltage (v_{pcc}).

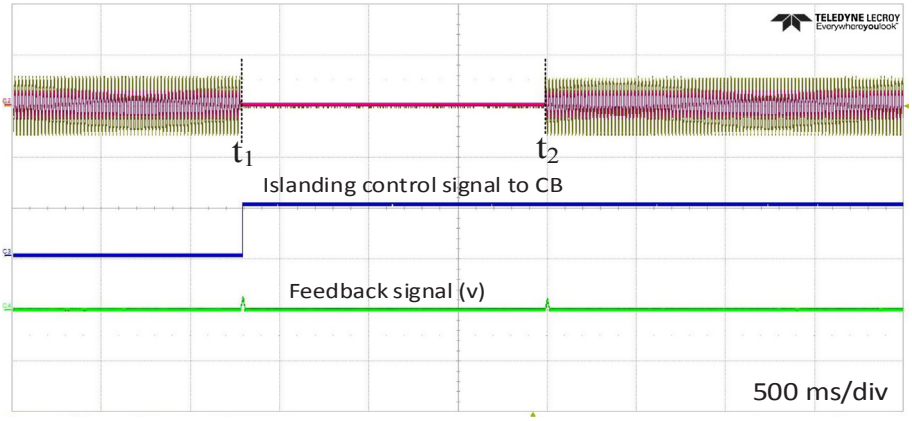

Fig. 14. Experimental results for islanding detection using second harmonics based PLL method: PCC voltage (v_g), grid current (i_g), islanding control signal to CB and feedback signal(v).

with phase margin (PM) of 47° under this mode. The overall loop gain [$G_{lgi}(s)$] is observed to be stable with PM = 69° under islanding conditions when k_{p1} = 0.5, as illustrated in Fig. 7(b). The overall loop gain under off-MPPT mode is also shown in Fig. 7(c). The change in the mode when k_{p1} = 0.5, will not affect the current control loop stability (PM = 39°) as shown in Fig. 7(c).

5. Results and discussion

5.1. Simulation results

Detailed simulation studies are carried out using MATLAB/Simulink software to verify the validity of the proposed control strategy. Some of the power management objectives defined in Section II are investigated under steady state and dynamic conditions.

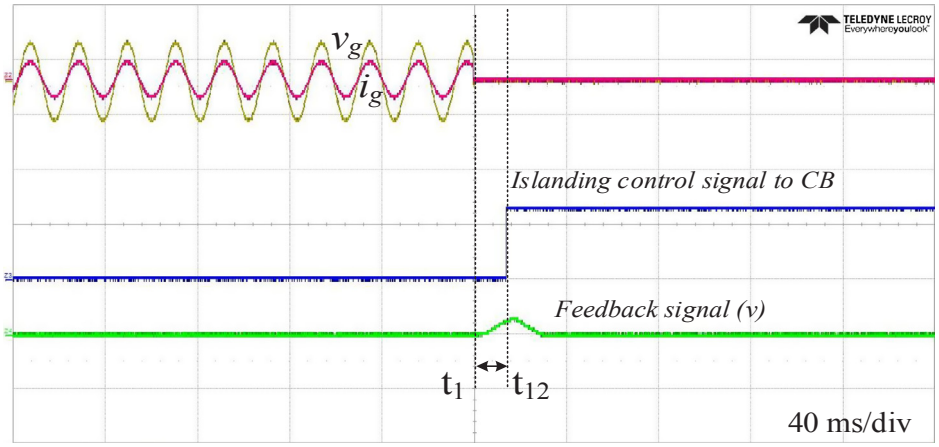

Fig. 15. Zoomed view of experimental results for islanding detection using second harmonics based PLL method: PCC voltage (v_g), grid current (i_g), islanding control signal to CB and feedback signal (v).

5.1.1. Performance of proposed scheme under grid connected and islanded modes

The steady state and dynamic performances of the proposed scheme under the grid interfaced/islanded conditions are illustrated in Fig. 8(a)–(g). From $t = 0$–1 s, the hybrid microgrid system is operating under grid interfaced mode and also, the renewable power is less than the load demand. As a result, the grid interfaced system operates in the deficit power mode. The battery units, PV system and utility grid share the total average load demand under steady-state conditions. The dynamic changes in the power during this mode are supplied/absorbed by the supercapacitor units. The grid side VSC provides a portion of the average load demand by drawing power from utility grid. In addition to this function, the harmonic and reactive components of the load current are supplied by the VSC as shown in Fig. 8(e)–(g). This ensures that the utility grid current is not only sinusoidal, but also in phase with the grid voltage. The corresponding changes in powers are also shown in Fig. 8(d).

The rms voltage and frequency of the utility grid is monitored and based on this signal, the islanded mode is activated at $t = 1$ s. The dynamic power changes during these transient conditions are supplied by the supercapacitor units and the battery supports the additional average demand to meet power balance at the DC grid as shown in Fig. 8(b). The DC link voltage is regulated by the battery and supercapacitor units during this dynamic transition.

During $t = t_1$–t_2 instants, the microgrid system operates in I-DPM. The entire AC and DC load demand during I-DPM is supported by the battery unit alone. As a result, the DoD of the battery unit rises to the middle level and this condition forces the load shed module activation at $t = 3$ s, as shown in Fig. 8. Due to the activation of the load shed module, 50% of the DC load is disconnected from the system and therefore, the battery storage system is relieved from discharging large power. During $t = t_2$–t_3 instants, the battery DoD reaches its upper limit. As a result, at $t = 5$ s, the load shedding module dispatches a signal to disconnect a portion of the AC side load.

Due to deactivation of the AC load, the power drawn from the grid side VSC and consequently, the power supplied by the battery storage system are reduced, as shown in Fig. 8(d). During $t = t_4$ instant, the power generated from the PV system is more than the load demand, and therefore, the microgrid system operates in I-EPM. The excess power during this mode is mainly utilized to charge the battery and the supercapacitor storage systems. Consequently, the peak power tracking deactivation module dispatches the control signal and the PV system operates at off maximum power tracking mode.

5.1.2. Voltage and power quality aspects of proposed scheme

The voltage and frequency at the AC load under islanded conditions are regulated by operating grid side VSC in voltage control mode (VCM). The main PQ functions provided by the proposed EMS under grid interface mode are current harmonic mitigation, reactive power support, load balancing and power factor improvement. The aforementioned PQ features are illustrated in Figs. 8,9.

5.2. Experimental results

A scale down test bed is developed in laboratory as shown in Fig. 10. A few of the power management objectives defined in Section II are investigated under steady state and dynamic conditions. The control switches used in the voltage source converter, battery, supercapacitor and RES converters are Semikron SKM 75GB128D. Amptek 6-DZM-14 (2 h) battery units with capacity of 12 V at 14 Ah each and Maxwell BMOD0058 E016 B02 supercapacitor units with capacity of 58 F at 16 V each are used as energy storage devices.

Chroma programmable power source is used to emulate the grid. Some of the obtained results are presented in the following paragraphs.

5.2.1. DC grid side performance

The dynamic performance of the proposed control strategy under DC load change is shown in Fig. 11. The transient part of the load change is supported by the supercapacitor and therefore, the variation in battery current during the dynamic conditions is less as shown in Fig. 11.

5.2.2. Performance under grid connected and islanding modes

The steady state and dynamic performance of the system are investigated under the following scenarios,

1. Grid connected mode,
2. Islanding mode,
3. Dynamic change over from one mode to another.

The steady state performance of the proposed control strategy under grid connected mode with a linear load is shown in Fig. 12. In this case, the load active power is shared by the utility grid and voltage source converter. The steady state performance of the proposed control strategy under islanding mode with a linear load is shown in Fig. 13. In this case, the entire load demand and losses in the microgrid are supported by the energy storage system. Also, grid current under this mode becomes zero as shown in Fig. 13.

The dynamic transfer between these two modes of the system is depicted in Fig. 14. The second harmonic based phase locked loop (PLL) method for the islanding detection was implemented in the experimental platform and the results obtained are shown below in Fig. 14.

The zoomed view of the experimental results at t_1 in Fig. 14 is shown in Fig. 15 for clarity. As shown in Fig. 15, the grid connection is disconnected at time instant t_1, the feedback signal is extracted from the voltage of the point of common coupling (PCC). When the grid is disconnected from the system, the feedback signal overshoots then the feedback signal reaches the preset threshold value for islanding detection and so the islanding control signal to the circuit breaker (CB) is triggered as shown in experimental result in Fig. 15. The islanding control signal is generated in less than half cycle after the grid is disconnected. The faster operation can be controlled by changing the threshold to the feedback signal. The experimental results show the effectiveness of the proposed method for the practical application in the microgrid systems for islanding detection.

The proposed method relies on the continuous injection of the signal to the inverter reference current to be generated. This affects the inverter in the negligible way when the grid is available. When the grid is not present in the system the extracted feedback voltage signal from the PCC gives the information about the grid impedance change, thus this results in effective islanding detection.

6. Conclusion

A control strategy is proposed for a grid interfaced and islanded hybrid ESS with a battery and supercapacitors as the energy storage devices. The frequency and voltage magnitude regulation at the point of common coupling are achieved under islanded conditions. The dynamic energy during transition from grid interfaced to islanding and vice versa is captured by supercapacitor pack and therefore, seamless transfer between both the modes is achieved. Further, the small signal average models of the system are developed to investigate the stability under various operating modes.

References

[1] Bindner H, Cronin T, Lundsager P, Manwell JF, Abdulwahid U, Baring-Gould I, Lifetime modelling of lead acid batteries; 2005.

[2] Cai W, Liu B, Duan S, Zou C. An islanding detection method based on dual-frequency harmonic current injection under grid impedance unbalanced condition. IEEE Trans Ind Inf 2013;9:1178–87. https://doi.org/10.1109/TII.2012.2209669.

[3] El-Khattam W, Sidhu TS, Seethapathy R. Evaluation of two anti-islanding schemes for a radial distribution system equipped with self-excited induction generator wind turbines. IEEE Trans Energy Convers 2010;25:107–17. https://doi.org/10.1109/TEC.2009.2026604.

[4] Faqhruldin ON, El-Saadany EF, Zeineldin HH. A universal islanding detection technique for distributed generation using pattern recognition. IEEE Trans Smart Grid 2014;5:1985–92. https://doi.org/10.1109/TSG.2014.2302439.

[5] Ge B, Wang W, Bi D, Rogers CB, Peng FZ, de Almeida AT, et al. Energy storage system-based power control for grid-connected wind power farm. Int J Electr Power Energy Syst 2013;44:115–22.

[6] Hajizadeh A, Golkar M, Feliachi A. Voltage control and active power management of hybrid fuel-cell/energy-storage power conversion system under unbalanced voltage sag conditions. IEEE Trans Energy Convers 2010;25:1195–208. https://doi.org/10.1109/TEC.2010.2062516.

[7] Hredzak B, Agelidis V, Demetriades G. A low complexity control system for a hybrid dc power source based on ultracapacitor-lead acid battery configuration. IEEE Trans Power Electron 2014;29:2882–91. https://doi.org/10.1109/TPEL.2013.2277518.

[8] Hredzak B, Agelidis V, Jang M. A model predictive control system for a hybrid battery-ultracapacitor power source. IEEE Trans Power Electron Mar. 2014;29:1469–79. https://doi.org/10.1109/TPEL.2013.2262003.

[9] Kamyab E, Sadeh J. Islanding detection method for photovoltaic distributed generation based on voltage drifting. IET Gener, Trans Distrib 2013;7:584–92. https://doi.org/10.1049/iet-gtd.2012.0507.

[10] Karimi H, Yazdani A, Iravani R. Negative-sequence current injection for fast islanding detection of a distributed resource unit. IEEE Trans Power Electron 2008;23:298–307. https://doi.org/10.1109/TPEL.2007.911774.

[11] Kim JH, Kim JG, Ji YH, Jung YC, Won CY. An islanding detection method for a grid-connected system based on the goertzel algorithm. IEEE Trans Power Electron 2011;26:1049–55. https://doi.org/10.1109/TPEL.2011.2107751.

[12] Li W, Joos G, Belanger J. Real-time simulation of a wind turbine generator coupled with a battery supercapacitor energy storage system. IEEE Trans Ind Electron 2010;57:1137–45. https://doi.org/10.1109/TIE.2009.2037103.

[13] Lu D, Fakham H, Zhou T, François B. Application of petri nets for the energy management of a photovoltaic based power station including storage units. Renewable energy Jan. 2010;35:1117–24.

[14] Mahmood H, Michaelson D, Jiang J. A power management strategy for pv/battery hybrid systems in islanded microgrids. IEEE J Emer Sel Topics Power Electron 2014;2:870–82. https://doi.org/10.1109/JESTPE.2014.2334051.

[15] Massoud AM, Ahmed KH, Finney SJ, Williams BW. Harmonic distortion-based island detection technique for inverter-based distributed generation. IET Renewable Power Generation 2009;3:493–507. https://doi.org/10.1049/iet-rpg.2008.0101.

[16] Merabet A, Ahmed K, Ibrahim H, Beguenane R, Ghias A. Energy management and control system for laboratory scale microgrid based wind-pv-battery. IEEE Transactions on Sustainable Energy 2016. https://doi.org/10.1109/TSTE.2016.2587828. pp. 1–1.

[17] Sedaghat B, Jalilvand A, Noroozian R. Design of a multilevel control strategy for integration of stand-alone wind/diesel system. Int J Electr Power Energy Syst 2012;35:123–37.

[18] Tedde M, Smedley K. Anti-islanding for three-phase one-cycle control grid tied inverter. IEEE Trans Power Electron 2014;29:3330–45. https://doi.org/10.1109/TPEL.2013.2278792.

[19] Vahedi H, Karrari M. Adaptive fuzzy sandia frequency-shift method for islanding protection of inverter-based distributed generation. IEEE Trans Power Delivery 2013;28:84–92. https://doi.org/10.1109/TPWRD.2012.2219628.

[20] Vahedi H, Noroozian R, Jalilvand A, Gharehpetian GB. A new method for islanding detection of inverter-based distributed generation using dc-link voltage control. IEEE Trans Power Delivery 2011;26:1176–86. https://doi.org/10.1109/TPWRD.2010.2093543.

[21] Velasco D, Trujillo C, Garcera G, Figueres E. An active anti-islanding method based on phase-pll perturbation. IEEE Trans Power Electron 2011;26:1056–66. https://doi.org/10.1109/TPEL.2010.2089643.

[22] Yafaoui A, Wu B, Kouro S. Improved active frequency drift anti-islanding detection method for grid connected photovoltaic systems. IEEE Trans Power Electron 2012;27:2367–75. https://doi.org/10.1109/TPEL.2011.2171997.

[23] Zhao C, He Y, MA C. Quantitative efficiency and temperature analysis of battery-ultracapacitor hybrid energy storage systems. IEEE Trans Sustainable Energy 2016. https://doi.org/10.1109/TSTE.2016.2574944. pp. 1–1.

[24] Zhu Y, Xu D, He N, Ma J, Zhang J, Zhang Y, Shen G, Hu C. A novel rpv (reactive-power-variation) antiislanding method based on adapted reactive power perturbation. IEEE Trans Power Electron 2013;28:4998–5012. https://doi.org/10.1109/TPEL.2013.2245512.